Incorporating charge transfer effects into a metallic empirical potential for accurate structure determination in $(ZnMg)_N$ nanoalloys

Pablo Álvarez-Zapatero, Andrés Vega[a], and Andrés Aguado[a,*]

Received Xth XXXXXXXXXX 20XX, Accepted Xth XXXXXXXXX 20XX
First published on the web Xth XXXXXXXXXX 200X
DOI: 10.1039/b000000x

We report the results of a combined empirical potential−Density Functional Theory (EP-DFT) study to assess the global minimum structures of free-standing zinc-magnesium nanoalloys of equiatomic composition and with up to 50 atoms. Within this approach, the approximate potential energy surface generated by an empirical potential is first sampled with unbiased basin hopping simulations, and then a selection of the isomers so identified is re-optimized at a first-principles DFT level. Bader charges calculated in a previous work [Corr. Sci. **124**, 35 (2017)] revealed a significant transfer of electrons from Mg to Zn atoms in these nanoalloys; so the main novelty in the present work is the development of an improved EP, termed Coulomb-corrected-Gupta potential, which incorporates an explicit charge-transfer correction term onto a metallic Gupta potential description. The Coulomb correction has a many-body character and is feeded with parameterized values of the *ab initio* Bader charges. The potentials are fitted to a large training set containing DFT values of cluster energies and atomic forces, and the DFT results are used as benchmark data to assess the performance of Gupta and Coulomb-corrected-Gupta EP models. Quite surprisingly, the charge-transfer correction is found to represent only a 6% of the nanoalloy binding energies, yet this quantitatively small correction has a sizable benefitial effect on the predicted relative energies of homotops. Zn-Mg bulk alloys are used as sacrificial material in corrosion-protective coatings, and the long-term goal of our research is to disclose whether those corrosion-protected capabilities are enhanced at the nanoscale.

1 Introduction

Zinc-magnesium alloys have been intensively investigated in the last decades due to their several industrial applications. Zn-rich compositions, on one hand, are useful as sacrificial coatings for corrosion protection of materials. As a specific example, the application of steel-based construction materials is largely dependent on the use of protective metallic coatings containing zinc. These coatings provide barrier and galvanic protection to the steel substrates employed in automotive, building, and other industries, improving durability and aesthetic properties of final products. Previous experimental research [1–3] has shown that the time for appearance of significant amounts of red rust was 3 times longer for samples coated with the Zn-Mg alloy as compared to a pure Zn coating. The improved properties of Zn-Mg alloys have been suggested to stem from the superior capability of Mg atoms on the surface to form a protective oxide layer, which is more insulating and stable than the ZnO layer that would be formed on pure zinc [2].

The effect of magnesium was most benefitial for the specific intermetallic compositions $MgZn_2$ and Mg_2Zn_{11}. Weight loss for such alloy coatings was up to 10-fold lower than for a pure zinc coating; the alloy coatings allowed to passivate the sample material in a chloride environment and limited the efficiency of oxygen reduction. On the other hand, Mg-rich alloys possess a good biocompatibility and similarity of its mechanical properties to those of the human bone tissue, which renders those materials as promising candidates for biomedical and implant applications [4,5].

There are numerous examples by now that demonstrate that the physical and chemical properties of a material can be drastically modified at the nanoscale. Therefore, it is interesting to investigate explicitly if the protective properties of Zn-Mg alloys, related to their chemical reactivity, can be enhanced at the nanoscale, and this constitutes indeed the long term goal of our research line on Zn-Mg nanoalloys. The properties of a nanoalloy generally show a strong and non-monotonous dependence on both cluster size and composition, as well as on the number of electrons, and one could envisage taking advantage of all those degrees of freedom to fine tune a desired property such as the resistance against corrosion. In our previous works on pure zinc clusters [6,7], we have already identified a peculiar property which might be a key factor in explaining why zinc-based materials offer a good protection

† Electronic Supplementary Information (ESI) available: Atomic coordinates (in xyz format and Å units) of the Global Minimum structures reported in this paper; optimal values of potential parameters; some technical details and additional figures that support some of the claims made in the main paper. See DOI: 10.1039/b000000x/

a Departamento de Física Teórica, Atómica y Óptica, University of Valladolid, Valladolid 47071, Spain; E-mail: aguado@metodos.fam.cie.uva.es

against corrosion. Specifically, the distance separating the outermost atomic shell from the remaining interior or core atoms is anomalously long as compared to typical interatomic distances, and the empty space thus generated in the subsurface region is strongly depleted of electrons, effectively protecting the core from environmental reagents. A preliminary report on Zn_xMg_{20-x} nanoalloys has suggested that alloying with magnesium might further improve these protection properties[8]. More specifically, we found that the local reactivity (quantified by atom-condensed Fukui functions) becomes homogeneous across the nanoalloy surface precisely for compositions close to the optimal ones ($MgZn_2$ and Mg_2Zn_{11}), thus explaining why those compositions are special: the uniform reactivity of the whole shell is expected to promote the formation of a uniform oxide crust of approximately constant thickness and containing a minimum amount of defects, both features being desirable for a protective external layer. To make further progress on this interesting problem and identify insightful reactivity trends, we need to substantially extend our studies to cover a wide range of nanoalloy sizes and compositions.

Structural characterization of nanoalloys as a function of size and composition is a prerequisite for a detailed understanding of their reactivity properties, but it requires an exhaustive computational sampling of the potential energy surface. Locating the Global Minimum (GM) structure of a nanoparticle is a laborious task, particularly so when dealing with nanoalloys, for which the GM structure depends not only on cluster size but also on chemical composition. For fixed size and composition, not only the geometrical structure of the atomic skeleton has to be determined, but also the preferred homotop (i.e. the most stable chemical ordering), which increases the complexity of the potential energy surface to be scanned as compared to homoatomic clusters. A well established strategy consists of performing an exhaustive sampling of the approximate potential energy surface provided by an empirical potential (EP) to quickly determine trial structures that are then reoptimized at a first-principles density functional theory (DFT) level, which has come to be known as EP-DFT approach[9]. In order for this approach to be successful, the EP model must provide a reasonably accurate account of atomic interactions.

Metallic nanoalloys, however, often show subtle electronic effects that are not explicitly described by the commonly employed EP models, which reduces the predictive power of EP-DFT approaches. Charge transfer phenomena, for example, become significant whenever the two types of atoms in the mixture have sufficiently different electronegativities, and can significantly affect the segregation/mixing chemical order preferences. To deal with this issue, Zhang and Fournier[10,11] proposed EP models containing a term that describes metallic cohesion plus a coulombic charge transfer contribution obtained through the electronegativity equalization method (EEM). Their results showed that mixing is enhanced by coulombic interactions in systems with a large electronegativity difference. Cerbelaud *et al.*[12] later proposed a refined model in which the electronegativity and hardness of each atom is coordination-dependent. The improved potential always located a more stable homotop than the bare metallic EP after DFT reoptimization. Incorporation of charge transfer effects was found to increase both the number of hetero-bonds and the number of gold atoms at the surface of Au-Ag nanoalloys.

Charge transfer phenomena were found to be important also in our preliminar report on Zn_xMg_{20-x} nanoalloys[8], with maximum Bader charges of about $+1.2e$ for Mg atoms and $-2.0e$ for Zn atoms. The substantial electrostatic energy associated with those charges was proposed as the main factor explaining the magic composition observed at 1:1 equiatomic ratio. It also explains the observation that Mg-Mg metallic bonding in the alloy is isotropic while Zn-Zn metallic bonding is more directional, because the charge transfer populates the $4p$ orbitals of Zn atoms. A significant observation from that work is that a bare metallic EP is not able to reproduce the correct energetic ordering of homotops. Therefore, in this work we will develop and present a new EP model, called Coulomb-corrected-Gupta model, that augments the usual Gupta potential description of metallic interactions[13–15] with an explicit ionic contribution to bonding arising from charge transfer. Opposite to the previous similar attempts mentioned above, the main novelty in our approach is the employment of Bader charges of *ab initio* quality rather than EEM-derived charges, which ensures that the EP reproduces the correct (DFT) charge transfer trends. The success and efficiency of the whole approach is based on a very accurate parameterisation which allows to predict the Bader charge on a given atom directly in terms of its coordination environment, without the need for expensive *ab initio* calculations. The several parameters of the potential are fitted to a large training set containing DFT values of nanoalloy energies and atomic forces, and an independent testing set of DFT results is used as a benchmark to assess the performance of the EP model. The potential is then employed to locate the GM structures of equiatomic Zn-Mg nanoalloys within an EP-DFT approach. The equiatomic composition ratio is chosen here because the homotopic problem is most acute for this specific composition, providing thus a stringent test for the newly proposed model.

The paper is organized as follows. As the Coulomb-corrected-Gupta model is shown here for the first time, a detailed exposition is justified, which we offer in Section II. Section III contains then a description of the GM structures of nanoalloys with up to 50 atoms, as well as their main electronic properties and an analysis of cluster stabilities. The physical factors determining the preferred chemical ordering, as well as those producing specially stable clusters, are iden-

tified and discussed. Several insightful conclusions, as for example a substantial strengthening of Zn-Zn bonds upon alloying due to charge transfer, will emerge from the detailed physical discussion. Finally, section IV summarizes all the relevant conclusions from our work.

2 Computational Methods

The EP-DFT method relies on a two-step procedure: first, a global optimization algorithm is employed to achieve a fast and wide scan for local minima on the approximate potential energy surface generated by an empirical potential (EP); subsequently, the most promising structures obtained for each size and composition are re-optimized at the Density Functional Theory (DFT) level. The reliability of this approach depends on the quality of the trial structures obtained during the global optimization in the first step. Since the DFT energies are obtained from a local optimization of trial EP structures, these should not be very dissimilar to the real ones; in other words, the EP should capture the physical behaviour of the real material at a reasonable level. Thus, the design of an EP model that accurately describes interaction energies in Zn-Mg nanoalloys is a prerequisite to production runs, and the most important advance in the present paper.

2.1 Gupta EP for metallic interactions

Since both Zn and Mg are metallic elements, the Gupta potential [13–15] is a sensible option to choose as a starting point, which is often employed in nanoalloy research. Within this approach, the total energy of a binary A_xB_{N-x} nanoalloy is written as a sum of atomic contributions $E_{i,\alpha}$, where $i = 1,...,N$ assigns a number label to each atom and α =A,B specifies the atomic species it belongs to (throughout this work, the label $(i\alpha)$ should be understood as a single compound label, but the specification of the atomic species α will be added only in those terms where it is needed). Each atomic contribution is in turn decomposed into an attractive band-energy many-body term $E^{\rm band}_{i,\alpha}$ and a repulsive pairwise contribution $E^{\rm rep}_{i,\alpha}$:

$$E(A_xB_{N-x}) = \sum_{(i\alpha)}^{N} E_{i,\alpha} = \sum_{(i\alpha)}^{N} (E^{\rm band}_{i,\alpha} + E^{\rm rep}_{i,\alpha})$$

$$E^{\rm band}_{i,\alpha} = -\left\{ \sum_{(j\beta)\neq(i\alpha)}^{N} \xi^2_{\alpha\beta} \exp\left[-2q_{\alpha\beta}\left(\frac{r_{ij}}{r^0_{\alpha\beta}} - 1\right)\right]\right\}^{1/2} \quad (1)$$

$$E^{\rm rep}_{i,\alpha} = \sum_{(j\beta)\neq(i\alpha)}^{N} A_{\alpha\beta} \exp\left[-p_{\alpha\beta}\left(\frac{r_{ij}}{r^0_{\alpha\beta}} - 1\right)\right],$$

where r_{ij} is the distance between atoms i and j, and $A_{\alpha\beta}, \xi_{\alpha\beta}, p_{\alpha\beta}, q_{\alpha\beta}, r^0_{\alpha\beta}$ are constants traditionally fitted to experimental bulk quantities. More specifically, the homo-atomic (AA or BB) parameters are fitted to properties of the corresponding elemental bulk crystal phases, such as lattice constant, cohesive energy and elastic constants. The hetero-atomic parameters may be fitted to alloy properties such as the dissolution energy of a single impurity, or rather be estimated as appropriate averages of the homo-atomic parameters. $r^0_{\alpha\beta}$ is a scaling factor for the interatomic distances. Usually, $r^0_{\alpha\alpha}$ is taken as the nearest-neighbor distance in the corresponding bulk metal.

Parameters fitted to bulk properties do not need to be transferable to the nanoscale, and thus their direct application to nanoparticles should be deprecated unless explicit transferability tests are reported. In recent work by our group [6,7], a novel, alternative methodology has been proposed to extract optimal Gupta parameters for homo-atomic clusters, and there we explicitly showed that the optimal parameters for pure zinc clusters are significantly different from those appropriate for bulk zinc. The optimal potential was able to locate new, unprecedented, GM structures for most zinc cluster anions that could be independently assessed through an explicit comparison to experimental photoemission spectra. Therefore, in the present work we will similarly try to train our potential models exclusively using *ab initio* data on small clusters.

2.2 Performance of the bare Gupta potential for Zn-Mg nanoalloys

The bare Gupta potential has been already tested in a preliminary report on the Zn_xMg_{20-x} nanoalloys [8]. It was found to correctly capture the main structural features of these nanoalloys, in particular the geometry of their atomic skeleton is in good agreement with DFT results. However, the potential was not able to locate the most stable chemical order patterns, i.e. it failed badly in the search for stable homotops. By analizing the electronic structure provided by DFT, the authors observed that charge transfer effects are not negligible. Charge transfer effects should promote mixing, increasing the number of Zn-Mg hetero-bonds. However, this charge transfer effect is absent from equation 1. The failure of the bare Gupta potential in identifying stable homotops was then tentatively traced back to its omission of the strong coulombic interactions originating from charge transfer.

A detailed analysis of the Bader atomic charges in Zn_xMg_{20-x} nanoalloys [8] showed that they can be accurately parametrised in terms of simple structural order parameters. This will be a very important result for our development of an improved potential in the next subsection, as it implies that atomic charges can be expressed as explicit functions of the distances r_{ij} and so they can be obtained "on-the-fly" during a geometry optimization or molecular dynamics run, *without the need for expensive ab initio calculations*. Therefore, we

summarize here the main findings on the environmental dependence of Bader charges.

As a general trend, Zn atoms acquire a negative charge (and Mg atoms a positive charge) in the nanoalloys, as expected from the electronegativity values of the two chemical species (the electronegativities of Mg and Zn are 1.31 and 1.65, respectively, in the adimensional Pauling scale[16]). The amount of charge transfer can be quantitatively very large, with maximum Bader charges of $+1.2e$ for Mg atoms and of $-2.0e$ for Zn atoms. The Bader charge of a given atom follows a simple trend as a function of the local coordination environment of the atom. Moreover, the chemical nature of that coordination environment plays a clear dominant role in determining the value of the Bader charge, while purely geometric factors such as the coordination number (i.e. the distinction between corner, edge, facet or core sites, for example) play only a secondary role.

The simplest order paramater that achieved an accurate parameterisation of Bader charges is the number of Zn-Mg hetero-bonds. An important ingredient here is the precise definition of coordination number. In a bulk crystalline sample, the atomic environment around each atom can be easily organized into coordination shells, each appearing at a well defined distance due to the translational symmetry of the crystalline lattice. In the small clusters studied here, however, there is a large dispersion in the interatomic distances about the mean value (more similar to the situation found in an amorphous material), and it is not convenient to employ an abrupt cutoff to decide whether two given atoms are first-neighbors or not. We have thus defined the number of A-B bonds, $N(\mathrm{Zn}-\mathrm{Mg})$, as a continuous real variable by using a hyperbolic tangent as a smooth cutoff function. The hyperbolic function is constrained so that the coordination number is equal to one for Zn-Mg distances shorter than $d_1(\mathrm{AB})$, and approximately equal to zero for Zn-Mg distances longer than $d_2(\mathrm{AB})$. $d_1(\mathrm{AB}) = 2.7$Å is the shortest Zn-Mg distance found in all the nanoalloys, while $d_2(\mathrm{AB}) = 3.3$Å is chosen to lie approximately at the middle point between the first and second atomic coordination shells. This way, our definition of coordination number incorporates information about the precise values of interatomic distances:

$$N(\mathrm{Zn}-\mathrm{Mg}) = \frac{1}{2}\left[-\tanh\left(4.1\left(r_{ij} - \frac{d_1(\mathrm{AB})+d_2(\mathrm{AB})}{2}\right)\right)+1\right] \quad (2)$$

The absolute value of the Bader charge on a given Zn (Mg) atom was found to smoothly increase as the number of Mg (Zn) atoms in its first coordination shell increases, allowing to estimate the atomic charge from the value of $N(\mathrm{Zn}-\mathrm{Mg})$[8]. Our generalized definition of coordination number is the key ingredient to obtain such a smooth quality fitting.

An even more accurate parametrisation was obtained with improved order parameters incorporating information about the total coordination number of each atom (thus discriminating between corner, edge, facet, and internal atomic sites, for example). The new order parameters continue to consider $N(\mathrm{Zn}-\mathrm{Mg})$ as the dominant term, but with a small admixture of the total number of bonds (the sum of homo-atomic and hetero-atomic bonds). The number of A-A and B-B bonds are now also needed, and they are defined by the same type of hyperbolic tangent function (equation 2), but with different limiting values of $d_1(\mathrm{AA})$, $d_2(\mathrm{AA})$, $d_1(\mathrm{BB})$ and $d_2(\mathrm{BB})$ (values of all these parameters are provided in the ESI†). The order parameters are then:

$$\begin{aligned}\beta(\mathrm{Zn}) &= N(\mathrm{Zn}-\mathrm{Mg}) - 0.2[N(\mathrm{Zn}-\mathrm{Zn})+N(\mathrm{Zn}-\mathrm{Mg})]+1.08\\ \beta(\mathrm{Mg}) &= N(\mathrm{Mg}-\mathrm{Zn}) + 0.2[N(\mathrm{Mg}-\mathrm{Mg})+N(\mathrm{Mg}-\mathrm{Zn})]-0.68,\end{aligned} \quad (3)$$

with the constant offsets having no physical relevance (they are added just to ensure that the order parameters remain positive and take similar values for Zn and Mg atoms). The relative weight and sign of the geometrical term are those leading to optimal order parameters (i.e. producing the smallest dispersion in the fitting of Bader charges as a function of β), and notice that the sign of this term is different for Mg and Zn atomic species. The new order parameters describe much better the local coordination dependence of the Bader charge for *both* Mg and Zn atoms, as demonstrated by a very small dispersion (around $0.03e$ on average) of the DFT-calculated Bader charges with respect to a quadratic polynomial fitting in terms of the order parameters[8]. In practice, this significant finding implies we have direct access to Bader charges of *ab initio* quality for each set of atomic coordinates, up to an error of $\pm 0.03e$, without the need for their explicit (expensive) calculation.

There remains just a final caveat: it is well known that Bader charges are additive, i.e. their sum exactly recovers the total molecular charge. Our numerical polynomial fitting, however, obviously does not *exactly* satisfy this constraint, despite being quite accurate. In practice, for the neutral clusters that will be the object of this work, we impose this constraint explicitly by correcting *a posteriori* the charges read off the numerical fitting:

$$Q_i \Rightarrow Q_i - \frac{\sum_i Q_i}{N}, \quad (4)$$

where N is the total number of atoms in the cluster. Imposing charge neutrality this way corrects the charges by an amount smaller than the dispersion of the fitting in all cases. In other words, the correction does not alter the charges within the accuracy of our fitting. In the rest of this paper, it will be understood that all charges are corrected to satisfy charge neutrality.

Coming back to the development of an improved EP model, it is obvious that the potential should contain an ionic interaction component in addition to the many-body metallic interactions, and the charges entering the coulomb interaction part

may now be easily chosen according to the local coordination environment of each atom in the alloy, with the confidence that they are of *ab initio* quality.

2.3 The Coulomb-corrected-Gupta model

The electrostatic interactions resulting from charge transfer must be included in the atomistic model in order to provide a trustworthy energy landscape. In the present work, this is achieved by augmenting the original Gupta potential with electrostatic monopole energy terms, which is the simplest option to start with. Our approach shares then formal similarities with previous works [11,12], but despite those similarities, we will show there are fundamental differences in our implementation.

Our electrostatic energy term includes a monopole-monopole pairwise Coulombic interaction and atomic self-energies representing the energy cost of charging the atoms:

$$E_{elec} = \sum_{(i\alpha)} \left(\sum_{(j\beta),j>i} J_{ij} Q_i Q_j + E_{self,(i\alpha)} \right), \qquad (5)$$

where Q_i is the net charge on atom i, $J_{ij} = \left(\frac{1}{2(\eta^0_{i\alpha}\eta^0_{j\beta})^3} + r_{ij}^3 \right)^{-1/3}$ is the screening function developed by Louwen and Vogt [17], and $\eta^0_{i\alpha}$ is the chemical hardness of atom i, species α. The screening function is computationally convenient in order to have an EP model without instabilities associated with possible divergences, and physically represents the fact that atoms have a finite spatial extension with a core electron density. The self-energy is expressed as a power series expansion in terms of the atomic charge [18,19]. For an isolated atom:

$$\begin{aligned} E^0_{self,\alpha} &= \chi^0_\alpha Q_\alpha + \eta^0_\alpha Q^2_\alpha + C^0_\alpha Q^3_\alpha + D^0_\alpha Q^4_\alpha + ... \\ \chi^0_\alpha &= \left.\frac{\partial E_{self,\alpha}}{\partial Q_\alpha}\right|_{Q_\alpha=0} \qquad \eta^0_\alpha = \frac{1}{2}\left.\frac{\partial^2 E_{self,\alpha}}{\partial^2 Q_\alpha}\right|_{Q_\alpha=0} \\ C^0_\alpha &= \frac{1}{6}\left.\frac{\partial^3 E_\alpha}{\partial Q^3_\alpha}\right|_{Q_\alpha=0} \qquad D^0_\alpha = \frac{1}{24}\left.\frac{\partial^4 E_\alpha}{\partial Q^4_\alpha}\right|_{Q_\alpha=0} \end{aligned} \qquad (6)$$

where α =Mg or Zn, and the zero superindex is used to denote isolated atom properties. χ^0_α is the electronegativity of the isolated atom, quantifying its ability for attracting and holding additional electrons. According to general DFT principles, $\chi^0_\alpha = -\mu^0_\alpha$, with μ the chemical potential. The chemical hardness η^0_α, on the other hand, quantifies the sensitivity of the chemical potential to changes in the number of electrons: the larger the hardness, the more reluctant the system is to accept or donate electrons. Cubic terms would represent the charge dependence of the hardness, and so on, so different levels of approximation are obtained by truncating the series at a given order.

For an atom-in-molecule, the self-energy expression has the same mathematical form, but effective expansion constants are used that include corrections due to the incorporation of the atom in a molecule (or crystal) [20]:

$$E_{self,(i\alpha)} = \chi^*_{(i\alpha)} Q_{i\alpha} + \eta^*_{(i\alpha)} Q^2_{i\alpha} + C^*_{(i\alpha)} Q^3_{i\alpha} + D^*_{(i\alpha)} Q^4_{i\alpha} + ... \qquad (7)$$

where $\chi^*_{(i\alpha)} = \chi^0_{(i\alpha)} + \Delta\chi_{(i\alpha)}$, $\eta^*_{(i\alpha)} = \eta^0_{(i\alpha)} + \Delta\eta_{(i\alpha)}$ and so on. The quantities $\Delta\chi_{(i\alpha)}$ and $\Delta\eta_{(i\alpha)}$ subsume the influence of molecular environment and connectivity on the electronegativity and hardness of each atom. The use of effective expansion constants, adapted to the molecular environment, is convenient to get a faster convergence for the series. The environmental effects $\Delta\chi_{(i\alpha)}$ etc. are in principle different for each atom (notice the explicit use of $(i\alpha)$ label as a subindex), as each atom will experience a different geometrical environment. In order to reduce the number of free parameters, however, in this work we will describe just an "average" environmental effect by constraining the expansion coefficients to be the same for all atoms of the same species:

$$E_{self,(i\alpha)} = \chi^*_\alpha Q_{i\alpha} + \eta^*_\alpha Q^2_{i\alpha} + C^*_\alpha Q^3_{i\alpha} + D^*_\alpha Q^4_{i\alpha} + ... \qquad (8)$$

Finally, placing 8 into 5 we get the full expression for the electrostatic energy, which corresponds to the change of the cluster total energy upon charge transfer, for a given set of atomic coordinates [11].

An obvious problem in previous practical implementations of this energy model has been that the atomic charges are not known *a priori* and are hard to calculate. So in previous computational applications of it [21,22], atomic charges were derived from the electronegativity equalization method (EEM) [23–25], which states that when molecules are formed the electronegativities of the constituent atoms should become equal, their common value coinciding with the molecular electronegativity χ_{cluster}. Atom-in-molecule values of the electronegativities can be obtained within this model by differenciating the expression of the energy:

$$\chi^{\text{AIM}}_{(i\alpha)} = \frac{\partial E_{elec}}{\partial Q_i} = \sum_{j\neq i} J_{ij} Q_j + \chi^*_\alpha + 2\eta^*_\alpha Q_i + \Theta(Q_i), \qquad (9)$$

where $\Theta(Q_i) = 3C^*_\alpha Q^2_i + 4D^*_\alpha Q^3_i + ...$ accounts for the higher order terms in the series. Notice that when all the $Q_i = 0$ the electronegativities retain their reference values, so the quantity χ^*_α should be understood as the electronegativity of a hypothetical atom which has been already placed into a molecular environment but which has not been allowed yet to exchange charge with its neighbors. Imposing the constraints $\chi_{\text{cluster}} = \chi^{\text{AIM}}_1 = \chi^{\text{AIM}}_2 = \cdots$ and the conservation of total charge ($Q_{\text{tot}} = \sum_i Q_i$), a system of linear equations results from

which equilibrium atomic charges Q_i and the molecular electronegativity χ_{cluster} can be derived. One important virtue of EEM-derived charges within the context of this empirical potential model, is that they can be self-consistently evaluated within the same model at a negligible computational cost. At this point, however, it is important to emphasize that imposing the equalization of atomic electronegativities is an *external addition* to the energy model provided by equation 5, i.e. just one possible way of implementing that equation into a practical method.

The principle of electronegativity equalization is a fundamental milestone in DFT, as it is exactly satisfied by the self-consistent delocalized electron density. In effect, the constancy of the molecular chemical potential ($\mu = \frac{\delta E[\rho(\mathbf{r})]}{\delta \rho(\mathbf{r})}|_v$) is automatically satisfied as μ enters the variational principle as a constant Lagrange multiplier to impose the conservation of the total number of electrons. But strictly speaking, DFT provides a sound value only for the electronegativity of the whole molecule, while the EP model of equation 5 requires a partition of the total system into atoms. If electronegativities of atoms-in-molecule are needed, one first has to define what an atom-in-molecule is, and there is not a unique definition within DFT for that concept. Therefore, DFT does *not* provide, at least in a uniquely defined way, all the input parameters required for an EEM application of equation 5. Additionally, this simplified energy model is written in terms of effective point charges, which can not represent all the complexity of the continuous density distribution of a DFT calculation. Previous work by Bultinck and coworkers[21,22] already showed that EEM-derived point charges are generally not compatible with well-established atomic charge definitions such as charges fitted to reproduce the electrostatic potential (CHELPG), or those based on Hirshfeld or Bader partitions of the total electron density. We emphasize that a DFT calculation produces both the "correct" electrostatic potential (i.e. within a given XC-approximation) *and* a constant chemical potential, for example, while the model of equation 5 can not satisfy both requirements. Failures like this one may be due to the functional form of equation 5 not being sufficiently flexible, to the point charge approximation truncated at the monopolar level, to the imposition of the EEM model to derive the values of the point charges, etc.

In the novel implementation of equation 5 employed in this work, we depart from the electronegativity equalization assumption because we have access to Bader atomic charges of *ab initio* quality at a cost which is even lower than that needed to derive EEM-charges. The Bader charges are directly obtained from atomic coordinates and could in principle be fed into equation 5. As the Bader charges are then explicit functions of atomic coordinates and so depend on local environment, the whole model (both Gupta and Coulomb parts) acquires a many-body character. The self-energy term retains its role as an effective repulsive many-body interaction resulting from charge transfer. This alternative use of the EP model given in equation 5 is, in our opinion, the main element of novelty introduced by our work. It guarantees that a part of the potential (the Coulomb part) is in correspondence with the charge transfer trends obtained from *ab initio* calculations, so it should improve the transferability and accuracy of the resulting model.

Next we have to implement this new idea into a practical method. The most naive approach, consisting of directly feeding the full Bader charges into equation 5, is not expected to work. Bader charges are extracted from a topological analysis of the continuous electron density function provided by DFT, and are at the very least delocalized over the finite spatial extension of a Bader basin, while the simple model of equation 5 replaces this complicated function with a set of point charges, each of them associated with a particular atom in the molecule. Moreover, our model is truncated at the monopolar level, i.e. it does not include point dipoles or quadrupoles, while the Bader analysis is not specifically constrained to minimize the basin-integrated values of those atomic multipoles. Therefore, despite being chemically meaningful, Bader charges alone do not recover the electrostatic potential V outside the electron distribution, for instance[26]; Bader atomic dipoles and quadrupoles would be also needed in order to obtain an accurate representation of V as a superposition of atom-centered potentials. As a practical solution that preserves the mathematical simplicity of our monopolar model, we choose to feed into equation 5 *scaled Bader charges*, $Q_i \Rightarrow \varepsilon Q_i$, where the scaling parameter ε is constrained to be the same for all atoms. This way, the charge transfer *trends* predicted by the Bader analysis are strictly preserved, and ε can be considered as an additional (in fact, the last) parameter in our potential model, to be fitted together with the rest of parameters as explained later in this section.

As atomic charges can not be uniquely defined, choosing one particular definition is partially also a matter of personal taste. At this point a pertinent question might be: why choosing Bader AIM charges at all if they need to be scaled to make them consistent with the model of equation 5? Our answer is that Bader charges are recognized as being chemically meaningful, applicable to both periodic and molecular systems, valid for both surface and buried atoms, and strongly rooted on general quantum-mechanical principles. Additionally, they are quite stable, i.e. little-dependent on basis set issues, and directly connected to the experimentally observable electron density distribution. It is true that charges obtained through electrostatic potential fitting (as, for example, CHELPG charges) might be thought to be better adapted for direct substitution into equation 5. But we have explicitly evaluated CHELPG charges for several Zn_xMg_{20-x} nanoalloys, and observed they are strongly dependent on the def-

inition of van der Waals radii for the constituent atoms, so very different sets of CHELPG charges could be obtained for the same nanoalloy, some of them even predicting an opposite charge transfer from Zn towards Mg atoms. In other words, they are quite useless for a metallic nanoalloy. The smooth and accurate parametrisation of atomic charges in terms of local atomic environment would have been impossible using CHELPG charges, while physically sound trends were clearly identified with the Bader charges. At least on average, the CHELPG charges were always found to be much smaller in absolute magnitude (by about 75%) than Bader charges, so we expect an approximate value of $\varepsilon = 0.25$ for the scaling parameter if the scaled Bader charges are to reproduce the correct electrostatic potential. We will see below that the optimal value of ε is very close to this estimation, which supports the whole approach. We admit that it is possible that some other charge scheme[26] might work as well within our model, but an explicit test of different atomic charge definitions is beyond the scope of the present work.

2.4 Parameterisation of the Coulomb-corrected-Gupta model

The complete potential employed in our work is just the sum of equations 1 and 5. Next we need to devise a method to obtain optimal values for the many parameters appearing in the total energy expression. The metallic part apparently contains a total of 15 parameters due to the existence of separate A-A, A-B and B-B interactions. Nevertheless, López and Jellinek[27] demonstrated that the r^0 parameters are indeed redundant and can be fixed to unity without any loss of generality. In order to avoid linear dependencies in parameter fitting, we thus fix those parameters to unity so that 12 independent parameters are needed in the metallic part of the potential. Quite obviously, the set of parameters that were optimal for the bare Gupta potential will no longer be useful after addition of the Coulomb part, so they need to be refitted. The Coulomb part contains 9 parameters, namely the values of χ^*_α, η^*_α, C^*_α and D^*_α constants for each atomic species and the scaling factor ε. The total number of parameters of our combined potential model thus adds up to 21.

Although one can in principle try a brute force approach and consider all parameters as free, we have instead decided to constrain the values of some parameters. Specifically, we choose to fix the values of χ^*_α for Zn (Mg) atoms to the *ab initio* values calculated for the homo-atomic Zn_{20} (Mg_{20}) neutral clusters:

$$\chi^*_\alpha = \chi_{\text{cluster}} = \frac{\partial E}{\partial Q} = \frac{1}{2}(I+A) \qquad (10)$$

where E is the cluster total energy, I is the ionization potential and A the electron affinity. This way we enforce that those two constants adopt physically reasonable values extracted from first-principles calculations, and so ensure that the average environmental effects on those response properties are correct. The choice of a cluster size of 20 atoms as reference is due to our interest in the size range $N = 2-50$, so we just chose a typical cluster size within that interval.

With these choices, a total of 19 free parameters remain. They are fitted to *ab initio* DFT properties calculated on a training set of 102 different atomic configurations of Zn-Mg nanoalloys. The training set includes several sizes in the range $N = 10-50$, different composition ratios, as well as a diverse selection of skeletal structures (including ordered and amorphous geometries) and chemical order patterns. Some configurations correspond to local minima (i.e. zero atomic forces) on the DFT potential energy surface, some others are distorted away from equilibrium. For those configurations corresponding to local minima, we enlarged the training set by adding both slightly expanded and contracted configurations (by homogeneously scaling atomic coordinates), so that the true number of atomic configurations is in fact larger than 102. The fitting involves varying the potential parameters to minimize the difference between EP and DFT values of both atomic forces and cohesive energies. The force matching procedure should result in potentials producing accurate geometries (both distances and angles). The inclusion of energies in the fitting plays important additional roles: on one hand, by including in the training set several compositions, we train the potential towards reproduction of excess energy trends; by including several structural isomers of the same nanoalloy, we guide the potential towards a correct energetic ordering of isomers (i.e. the hierachy of local minima on the energy landscape); finally, introducing contracted and expanded configurations about a local minimum (an analog of pressure-volume curves in the bulk limit), we ensure the potential will reproduce at least the frequency of the average breathing vibrational mode and the system's compressibility. The optimization is performed by using a simplex downhill method.

An interesting outcome of the fitting is that inclusion of the *ab initio* compressibility tightly fixes the value of the scaling parameter to $\varepsilon = 0.28$, i.e. about the same as the ratio between CHELPG and Bader charges. No other value can reproduce the volume dependence of the energy despite the many other parameters involved in the fitting. It is both interesting and reassuring that the ε value needed to reproduce the compressibility is about the same as that required to produce a correct electrostatic potential.

The optimal parameters emerging from the fitting procedure, both for Gupta and Coulomb-corrected-Gupta potentials, are provided in the ESI†. Following the conclusions of our previous work, in the production runs we have employed ten additional potentials with parameters in a local neighborhood around the optimal ones, in an attempt to enhance structural diversity. The quality of the fitting is about equally good

for all these eleven potentials as they are all close to the optimal values.

The training error provides a first glimpse at the relative performance of the two EP models. We have also generated a testing set with over 700 structures which were not used in the fitting but were evaluated at the DFT level as a result of the optimizations performed in this work. At a quantitative level, the mean absolute error in the testing system is approximately three times bigger than in the training system, yet both training and testing errors show the same qualitative trends. The mean absolute errors of the bare Gupta potential in the testing set are around 0.15 eV/atom for cluster binding energies and 0.5 eV/Å for the atomic forces. These errors may be considered big at first sight, but we stress that the testing set contains over 700 clusters sampling a very wide region of configuration and homotopic spaces, and tests as complete as the present one are scarce in the previous literature. The Coulomb-corrected-Gupta model reduces these errors by around 5% compared to the bare Gupta errors, which is not a very significant improvement at a quantitative level. In fact, the charge-transfer contribution to the energy (eq. 5) is a mere 6% of the total binding energy, i.e. around the same as the percentage improvement in the fitting error.

As a conclusion of this section, the charge-transfer effects do not seem to constitute the dominant correction to the bare Gupta potential description, as it had been hypothesized based on the large values of Bader charges. Although this is somehow a "negative" conclusion of our work, we believe it is a significant finding that may guide future studies. The small size of the effect is traced back to scaling down of the original Bader charges by $\varepsilon = 0.28$, a scaling that is strictly necessary to reproduce the right curvature of the potential energy surface around local minima. We doubt that inclusion of higher-order multipolar effects such as charge-dipole, dipole-dipole or charge-quadrupole interactions could significantly improve the fitting error; we rather suspect it is the metallic part of the potential which needs to be improved to efficiently reduce the fitting error. We emphasize that the charge-transfer correction here described could be implemented together with any other potential describing metallic interactions, so it may be useful within that wider scope. We will also show in this paper that the apparently small 6% charge-transfer contribution is enough to significantly improve the relative energetics in homotopic space, and in this sense it is also a worthwhile contribution.

2.5 Technical details of the EP-DFT protocol

We have implemented the Coulomb-corrected-Gupta potential into a module of the freely available GMIN code[28], with which we perform Basin Hopping (BH) global optimizations[29,30]. For each nanoalloy of fixed size and composition, we perform three independent BH runs (each 500000 steps long) for each of the 11 potentials available. This adds up to a total of 33 BH runs, or 18 million BH steps, for each nanoalloy. Each BH step may be of two kinds: either a random change of all atomic coordinates, or a swap move exchanging the chemical identity of a randomly chosen A-B pair of atoms. The percentage of swap moves in the BH runs is of 20%. The three runs for each potential differ just in the specific temperature value employed in the Metropolis Monte-Carlo acceptance step during the BH optimization. Additionally, if no lower energy structure is identified during 50.000 consecutive steps, the cluster structure is re-seeded to a random one in order to enhance sampling. The best 100 structures from each run are stored and merged together to form an initial databank of trial structures. This databank is further enlarged by performing additional BH runs with only swap moves on the 10 more stable structures identified by each potential, thus obtaining a more complete sampling of homotopic space.

The initial database so constructed may easily contain duplicate structures, because both the energy and the detailed geometry of a given structural isomer are not directly comparable between different potentials. So our next step is to apply a filtering process that removes duplicates from the databank. As explained in the ESI†, we have devised a structural descriptor function, based on the distribution of pair interatomic distances, that is able to identify similar structures, where the "degree of similarity" can be quantitatively defined by the user. The descriptor is very robust in removing duplicates. Being based purely on pair distances, it does not depend on the global orientation of the cluster or on permutations of identical atoms, and automatically removes enantiomers in case of chiral structures. Finally, after removal of duplicates, we select a final list of 100 structures to feed the DFT reoptimization process. The selection process involves a balance of stability and diversity factors: half of the list is formed by the most stable structures found in the BH runs; for the other half, we use again our structural similarity descriptor to choose a set of candidates which is as diverse as possible. With this choice, highly symmetric structures are usually selected for re-optimization.

Next, we re-optimize locally the selected structures at the Kohn-Sham density functional theory (KS-DFT) level, employing the SIESTA code[31]. Exchange-correlation effects are treated within the generalized gradient approximation of Perdew, Burke and Ernzerhof (PBE)[32], and norm conserving pseudopotentials are used to describe the effect of core electrons[33,34]. The semicore 3*d* states of zinc are explicitly included in the active valence space. Our pseudopotentials include non-linear partial core corrections[35] which are known to be important for both zinc and magnesium. A basis of localized atomic orbitals is employed to expand the wave function of the cluster. In our calculations, the size of the basis set was

double-zeta plus two polarization orbitals (DZP2), resulting in a total of eight basis functions per Zn atom and six basis functions per Mg atom. The clusters are placed in a cubic supercell with a length of 30 Å to make the interaction between periodic images negligible. Equilibrium cluster geometries are then obtained from unconstrained conjugate-gradients structural relaxation using DFT forces. The structures were relaxed until the force on each atom was smaller than 0.01 eV/Å. In our previous work on pure Zn clusters [7], we provided extensive benchmark tests demonstrating the accuracy of these computational settings.

3 Results and Discussion

3.1 Homotop energetic ordering in Zn_xMg_{20-x} nanoalloys

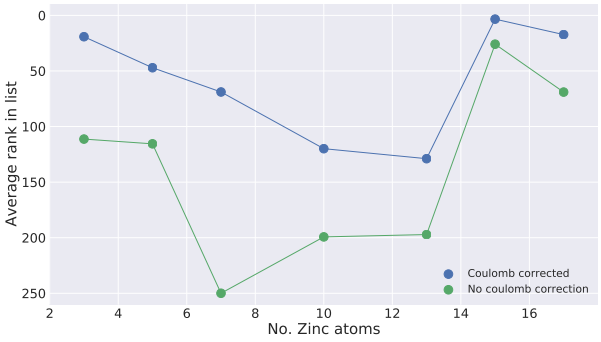

Fig. 1 Assessment of the performance of bare and Coulomb-corrected Gupta models in predicting homotop stability. The test is performed on Zn_xMg_{20-x} nanoalloys in the whole range of chemical compositions. See main text for details.

Zn-Mg nanoalloys with $N = 20$ atoms and all possible compositions were studied in detail in our previous work [8]. We explicitly relaxed up to 500 different homotops explicitly at the DFT level for $x = 7 - 13$, in order to have some confidence about the putative GM homotops. Here we take advantage of the extensive *ab initio* data bank generated in our previous work to test the performance of the Coulomb-corrected-Gupta model in predicting homotop relative energetics for selected values of x, covering the whole range from dilute to equiatomic compositions. We have conducted BH optimizations with only swap moves to sample the homotopic space of the GM atomic skeleton in 500000 BH steps, and stored the 250 most stable homotops located by each potential, both with and without charge-transfer corrections. In first place, we have explicitly checked that none of the new homotops generated in these searches is more stable than the putative GM already reported. Then, in order to rank the several potentials, we have just looked at the position that the DFT global minimum homotop occupies in the list of energy-ordered homotops predicted by each potential. As we are using eleven different potentials for both the bare and the Coulomb-corrected models (see previous section), we show in figure 1 the position of the DFT GM averaged over the 11 potentials. When the average rank is higher than 250, we just set it to 250 when producing this plot.

Figure 1 clearly demonstrates that the apparently small (6%) charge transfer contribution to the binding energy produces a substantial improvement in the description of chemical order in Zn-Mg nanoalloys, and does so systematically for all compositions. The results of this test for $x = 7$ are very revealing: none of the bare Gupta potentials is able to position the correct (DFT) homotop among the 250 most stable predicted homotops, so quite obviously the right homotop would be missed by a BH search based on this potential; however, the coulomb-corrected-Gupta potentials find on average the DFT GM within their 60 most stable structures, and the best potential does so within the 45 most stable structures. The improvement is very significant and it is self-evident that the chances to locate the correct GM substantially increase when using the improved potential. For equiatomic ratio $x = 10$, which is the most complicated case, the average rank of the Coulomb-corrected model over the 11 different potentials is 120, which might be considered a high rank, but if we remember that there may be up to $\binom{20}{10}$=184756 different homotops, the result is quite good indeed, and we aditionally notice that the best Coulomb-corrected potential locates the right isomer within the 30 most stable homotops.

In summary, this test demonstrates that the improved description of chemical ordering provided by the new EP model is transferable to all nanoalloy composition ratios, a highly desirable feature in nanoalloy research. In the ESI†we provide additional tests carried on a 79-atom truncated octahedron, that demonstrate that the improved description of chemical order is transferable to cluster sizes well outside the size range employed in the fitting procedure.

3.2 Putative Global Minimum Structures for equiatomic nanoalloys

The putative GM structures located in this work are shown in figures 2 and 3. We discuss the nuclear skeleton geometries first. In general terms, they are quite similar to those obtained for pure Zn clusters in previous works . Mg_2Zn_2 adopts a tetrahedral shape, and the structures of clusters with 6 and 8 atoms are based on glueing several tetrahedral units together. Nanoalloys in the size range $N = 10 - 16$ are rather based on a tri-capped trigonal prism unit (TTP) as the fundamental building block. The TTP unit is in fact the GM structure of Zn_9 . Zn_5Mg_5 and Zn_6Mg_6 display one and three adatoms, re-

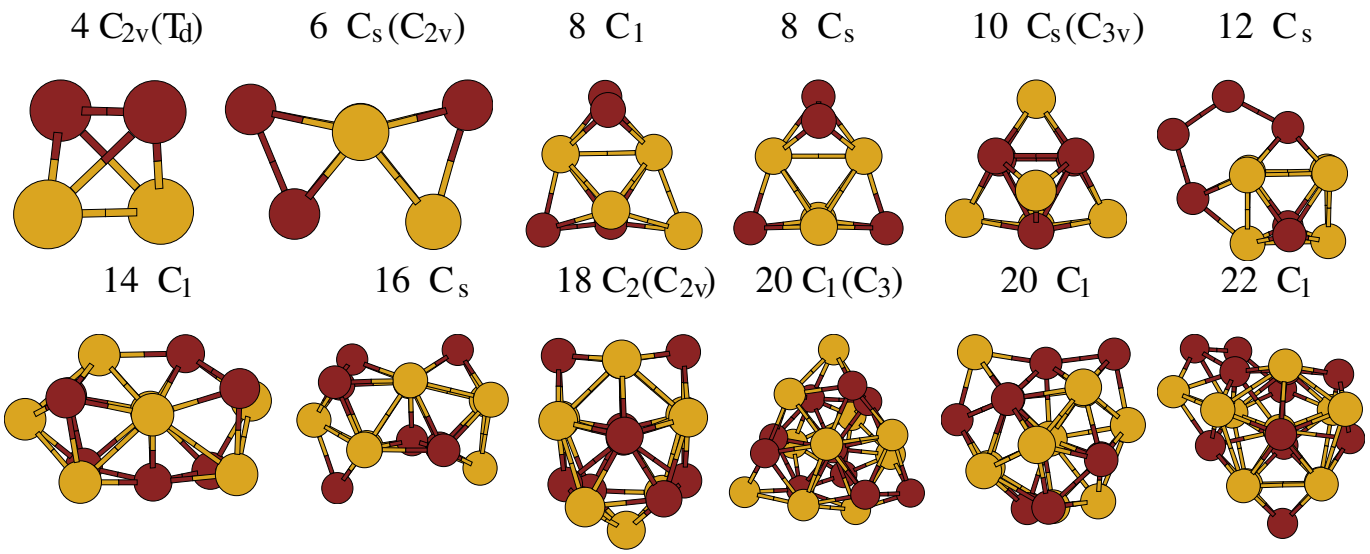

Fig. 2 Putative GM structures and approximate point group symmetries of equiatomic Zn-Mg nanoalloys with $N = 4-22$ atoms. Brown and golden spheres represent Zn and Mg atoms, respectively. For some clusters, we add in brackets the point group symmetry of the corresponding homo-atomic cluster in order to better appreciate the symmetry of the structure. More than one structure is shown in case of near-degeneracy.

spectively, on the surface of one TTP unit, while Zn_7Mg_7 and Zn_8Mg_8 contain two TTP units that share some atoms. Up to this size the clusters have no internal or core atoms. Nanoalloys with $N = 18-22$ atoms contain a single core atom and are mostly based on a distorted 13-atom decahedron with adatoms around its equatorial waist, although for $Zn_{10}Mg_{10}$ a twisted pyramidal structure (which is the GM for both Zn_{20} and Mg_{20}) is degenerate with the distorted decahedral isomer.

Clusters in the size range $N = 24-28$ have two core atoms and so display an elongated global shape. The GM structure of $Zn_{12}Mg_{12}$ is highly symmetric, as it can be viewed as a relatively small C_{2v} distortion of a D_{4h} structure, and displays a series of stacked alternating Zn/Mg planar layers. The same layers, although not so planar, can be clearly identified in the C_{3v} GM structure of $Zn_{13}Mg_{13}$, which is also a very symmetric structure based on two interpenetrating Frank-Kasper Z16 polyhedra. $Zn_{14}Mg_{14}$ follows the same trend, although adding two atoms appreciably distorts the structure. The nanoalloys with $N = 30, 32$ atoms contain three core atoms in a triangular arrangement and an oblate shape. They are quite ordered both structural and chemically: the shell of $Zn_{15}Mg_{15}$ is perfectly decahedral, for example.

Clusters with $N = 34, 36$ contain a 4-atom tetrahedral core. $Zn_{17}Mg_{17}$ has a global tetrahedral shape which is the same as the GM structure of Zn_{34} , and a highly symmetric C_{2v} chemical ordering once more based on alternating "layers" of Zn and Mg atoms. Adding only two atoms produce a completely amorphous structure for $N = 36$. Clusters with $N = 38-42$ contain five core atoms forming a trigonal bi-pyramid; for $N = 44$ the core has six atoms in a severely distorted trigonal prism configuration; finally, sizes $N = 46-50$ contain seven core atoms. Nearly all of these clusters are quite amorphous, the exceptions being $N = 38$ and $N = 46$. $Zn_{19}Mg_{19}$ has almost C_2 symmetry and displays a clear stacking of Zn and Mg layers. Concerning $Zn_{23}Mg_{23}$, its core is a capped octahedron with C_{3v} symmetry which itself displays the alternating Zn/Mg chemical order. The shell is decahedral, with a rounded shape and also quite symmetric, but core and shell are not congruent enough to produce a high global symmetry.

We discuss chemical order trends next. There are three important factors that determine the tendency towards segregation or mixing in Zn-Mg nanoalloys: (1) the bulk cohesive energy of Mg is 12% larger than that of Zn. Assuming that the relative strength of Mg-Mg and Zn-Zn bonds is maintained in the nanoalloys, this factor would tend to maximize the number of Mg-Mg bonds, and so would favor Mg@Zn segregation; (2) interatomic distances in bulk Mg are around 30% longer than in bulk Zn, implying a considerable size mismatch between both elements. In order to minimize bond strain, the small element tends to segregate to the cluster core, so this factor alone would favor Zn@Mg segregation. As the two factors oppose each other, segregation trends are not clear and our calculations show that already a bare Gupta potential favors mixed nanoalloys, with the mixing being quite random in nature as in a bulk solid solution; (3) finally, charge transfer effects introduce an ionic bonding component that tends to maximize the number of Zn-Mg bonds and thus promotes mixing. In fact, the Coulomb-corrected-Gupta potentials pre-

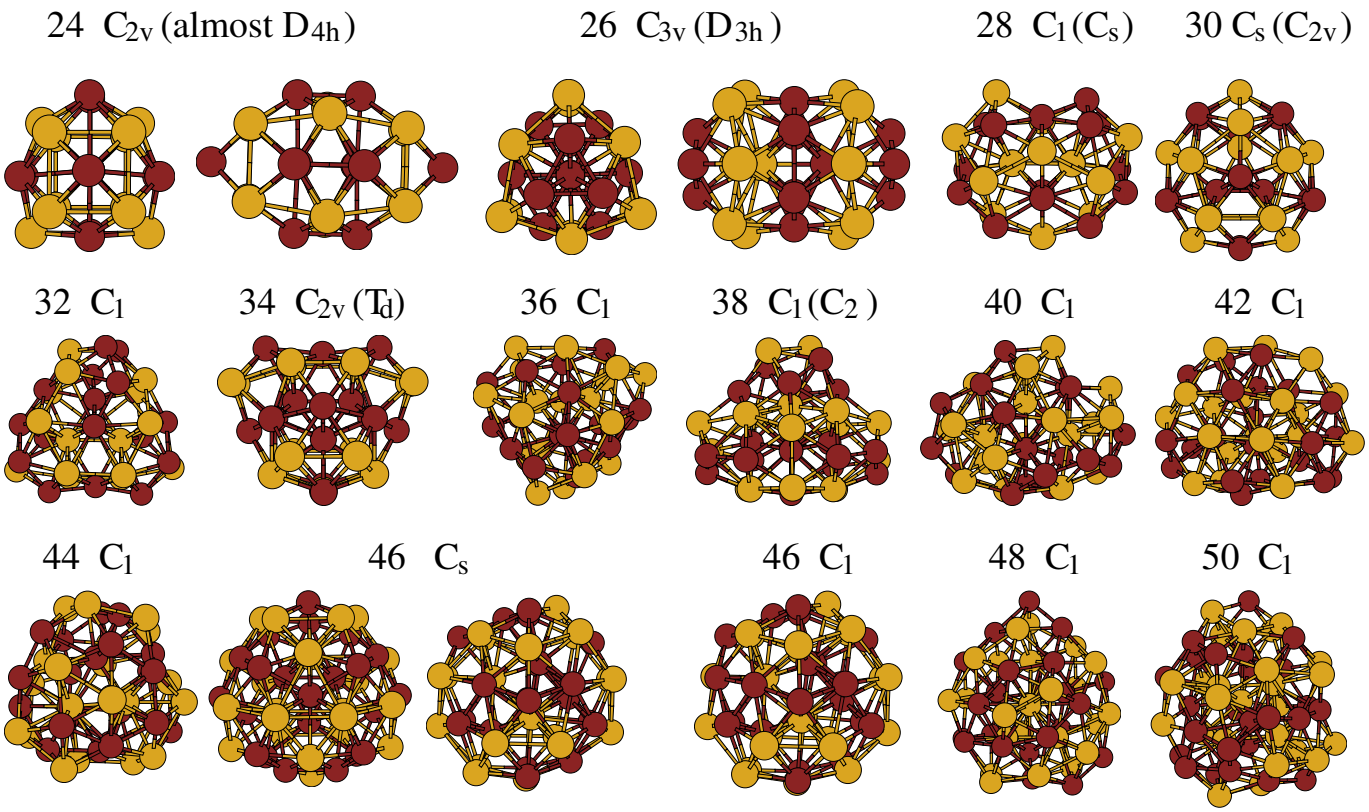

Fig. 3 Putative GM structures and approximate point group symmetries of equiatomic Zn-Mg nanoalloys with $N = 24 - 50$ atoms. Front and side views of the same cluster are shown for some highly symmetric structures. Rest of the caption as in Figure 2.

dict also mixed structures, but with the important addition that the mixing is not so random in nature, as chemically ordered nanoalloys more similar to intermetallic bulk phases are stabilized compared to bare Gupta predictions. Moreover, a significant amount of charge transfer can modify the conclusions extracted from the other two arguments and reinforce mixing through an "indirect" mechanism. In fact, as Mg atoms donate electrons to Zn atoms, the effective size of a Zn atom in the nanoalloy is expected to increase as compared to the same size in a pure zinc cluster, while the size of Mg atoms will decrease, thus charge transfer reduces the size mismatch. Similarly, we expect that the metallic Mg-Mg bonding is weaker in the nanoalloy as compared to a pure Mg cluster, because Mg atoms embedded in the nanoalloy have on average missed one electron, and so there are less electrons available for direct Mg-Mg bonding. Similarly, the metallic part of the Zn-Zn bond strength will be enhanced in the nanoalloy through the directional bonding expected between the acquired electrons which populate the $4p$ orbital of Zn. These effects have been already observed in simulations of the Laves phase of $MgZn_2$ [36], a material displaying isotropic Mg-Mg bonding but directional Zn-Zn bonding due to the charge transfer. The essential message here is that, when the charge transfer is important, an atom in the nanoalloy may be quite a different object as compared to the same atom in the pure metal.

A direct visualization of figures 2 and 3 already shows that Mg and Zn atoms are well mixed in the equiatomic nanoalloys, and for $N > 22$ additionally show a tendency towards compositional layering. In order to quantify the degree of mixing, we have evaluated the following mixing indicator for each of the GM structures:

$$p_{\rm mix} = \frac{N_{\rm AB} - N_{\rm AB}^m}{N_{\rm AB}^M - N_{\rm AB}^m}, \qquad (11)$$

where $N_{\rm AB}$ is the number of Zn-Mg bonds, evaluated as explained in the methods section. $N_{\rm AB}^M$ and $N_{\rm AB}^m$ are respectively the maximum and minimum values that $N_{\rm AB}$ can take for that particular *frozen* nuclear skeleton. These two last numbers are obtained from swap-only BH runs without allowing for structural relaxation. The parameter thus defined is normalized between zero and one, with a value $p_{\rm mix} = 1$ indicating the maximum degree of mixing that a given nuclear skeleton allows. The value $p_{\rm mix} = 0$ is always obtained for left-right segregated structures, displaying an approximately flat interface separat-

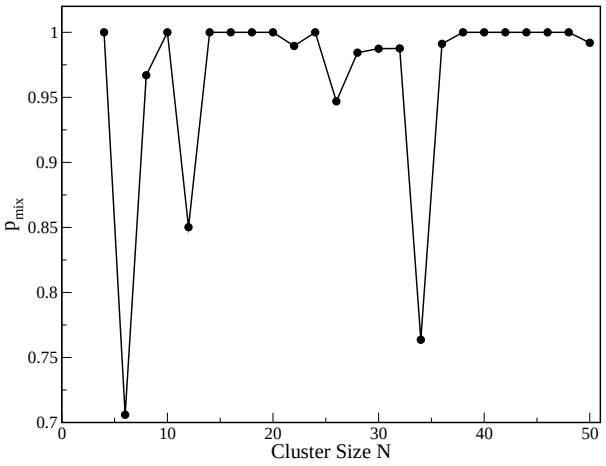

Fig. 4 The mixing parameter is shown as a function of the size of the nanoalloy.

ing pure zinc from pure Mg sides. Figure 4 demonstrates that many Zn-Mg nanoalloys are indeed maximally mixed, and more in general all of them display a high degree of mixing. It is particularly interesting that the perfect compositional layering observed in $Zn_{12}Mg_{12}$ produces a maximally mixed homotop, in which any Zn-Mg swap would decrease the number of Zn-Mg bonds. All in all, figure 4 demonstrates that N_{AB} is the dominant parameter determining the most stable chemical order, even if nanoalloys with $N = 6$, 12 or 34 atoms are notable exceptions that prove the correlation between N_{AB} and homotop stability is not perfect.

In the following, we try to identify the secondary factors that influence homotop stability, by focusing on finer details of the chemical order. Nanoalloys with $N < 18$ have no internal atoms and so we expect that steric effects arising from size mismatch do not significantly affect the chemical ordering. In fact, we observe that the number of Mg-Mg bonds (N_{BB}) is the relevant parameter that competes with maximization of N_{AB} in determining the most stable homotop. Clusters with $N = 6, 8, 12$ atoms are not maximally mixed because they become stabilized by the larger cohesion of Mg-Mg bonds. For example, the C_s isomer of Zn_4Mg_4 contains a pure Mg_4 tetrahedron with external Zn adatoms; similarly, Zn_6Mg_6 contains a trigonal prism unit exclusively made up of Mg atoms. In general, we observe a higher connectivity between Mg atoms for all the small clusters with the only exception of Zn_5Mg_5, for which the GM is a maximally mixed homotop presenting a larger number of Zn-Zn bonds. We will rationalise this exceptional size in the next sections by relating it with a larger degree of charge transfer.

In nanoalloys with a core@shell structure we observe that the compactness of the atomic skeleton becomes a more important factor than the number of Mg-Mg bonds, and the compactness degree is mainly determined by the size mismatch. In fact, we observe a clear systematics in the evolution of the composition of the core as a function of size, that can be easily interpreted in terms of the size mismatch effect. For each core size (which is stable over a certain interval of cluster sizes) we observe that the core starts being Zn-rich at the beginning of the stability interval of that core size, and evolves towards a Mg-rich core at the end of the stability interval. So, as the core size increases, the nanoalloys fluctuate between Zn-rich and Mg-rich core compositions. For example, Zn occupies the single core site for $N = 18$ and the pyramidal isomer of $N = 20$, but it is Mg that occupies the core site for the decahedral isomer of $N = 20$ and for $N = 22$; the core evolves from Zn_2 to ZnMg and finally to Mg_2 for sizes, $N = 24, 26$ and 28, respectively; for $N = 34$ the core is a pure Zn_4 tetrahedron, while it becomes Zn_2Mg_2 for $N = 36$, etc. There are no exceptions to this systematic rule. The reason why $Zn_{17}Mg_{17}$ is not maximally mixed, for instance, is precisely its strong preference for a pure Zn core.

In order to demonstrate the importance of compactness arguments in determining the optimal core compositions, we focus on the so-called inverted homotop, which is obtained from each GM by a complete swap of all Zn and Mg sites. For equiatomic nanoalloys this chemical inversion does not modify the global composition. Notice that with our definition of the p_{mix} parameter (implying a rigid atomic skeleton), the inverted homotop has exactly the same value of N_{AB} and so the same p_{mix} as the GM homotop, so if N_{AB} were the only relevant parameter, the two homotops should be degenerate. Upon structural relaxation, however, we observe that the inverted homotop systematically expands, i.e. its mean square radius increases, so it is less compact (and usually quite less stable) than the GM homotop. We also notice that, once relaxed, the inverted homotop has a lower value of N_{AB} than the original GM homotop, as our definition of coordination numbers is distance-dependent. We have also checked that the mean square cluster radius increases upon modifying the core composition in the GM structures, so we can conclude that the optimal core composition is the one that makes the cluster most compact. For some sizes as for $N = 34$, this trend competes with the maximal mixing rule, producing a pure zinc core.

There is another interesting observation extracted from this analysis. The inverted homotop has all A-A bonds transmuted into B-B bonds and viceversa, as compared to the GM homotop. While most small clusters with no core atoms tend to prefer the homotop with maximum N_{BB}, for the cluster with 10 atoms and for several of the bigger size nanoalloys the GM homotop has more A-A bonds than the inverted homotop, i.e. these clusters tend to maximize the number of Zn-Zn contacts instead. As we will show in the next sections, these clusters

display a higher than average amount of charge transfer, so we can conclude that the amount of charge transfer modulates the relative strength of Zn-Zn and Mg-Mg bonds, as suggested in the tentative arguments provided above. Quite obviously, this effect renders the detailed chemical ordering preferences size dependent and so quite unpredictable.

In summary, chemical order preferences in equiatomic Zn-Mg nanoalloys are mainly dictated by a maximization of hetero-atomic bonds; exceptions to this rule arise whenever a homotop exists which is significantly more compact than the maximally mixed homotop, and size mismatch effects then tend to determine the composition of the core. For very small clusters, maximization of the Mg-Mg bonds seems to be a secondary factor to consider. While maximization of Zn-Zn bonds becomes preferred in systems with an enhanced charge transfer. Furthermore, we observe that charge transfer effects tend to enhance compositional layering.

To the best of our knowledge, there are no experimental results available for Zn-Mg nanoalloys that we could use to assess our results, which thus remain as purely theoretical predictions. Concerning the bulk limit, the equiatomic alloy is not reported as a stable intermetallic phase [37,38]. However, there is an intermetallic compound experimentally reported at close to equiatomic composition, namely $Mg_{21}Zn_{25}$, and another one, $Mg_{12}Zn_{13}$, has been predicted through computational thermodynamics calculations of the phase diagram [39], although this last one has not been experimentally characterized. Finally, DFT calculations for equiatomic composition [40] have reported a metastable orthorhombic phase with Pmma crystal group, which would decompose into $Mg_{21}Zn_{25}$+$Mg_{149}Zn$. It is a very interesting finding that our GM for $Zn_{12}Mg_{12}$ can be directly obtained by relaxing a fragment of the Pmma bulk lattice, so it can be considered a bulk fragment (we show in the ESI†images of that bulk phase and of the 24-atom relevant fragment). Similarly, $Zn_{13}Mg_{13}$ can be viewed as a fragment of the trigonal $Mg_{21}Zn_{25}$ lattice ($R\bar{3}c$ symmetry), although with a slightly different chemical ordering due to the different composition ratio. We suggest that the interpenetrating Z16 Frank-Kasper polyhedra in $Zn_{13}Mg_{13}$ might be a candidate building block for the still unassigned $Mg_{12}Zn_{13}$ crystal phase, given the proximity in composition and also in the total number of atoms per formula unit.

3.3 Electronic Properties

We have evaluated the vertical ionization potential (IP) and electron affinity (EA) of all GM structures through a $\Delta-$SCF calculation, i.e. by explicitly calculating the cation or anion state at the optimal geometry of the neutral cluster and taking the appropriate difference of total energies. We have also evaluated the fundamental gap, defined as E_{gap}=(IP-EA), which is twice the chemical hardness. The numerical values of all these

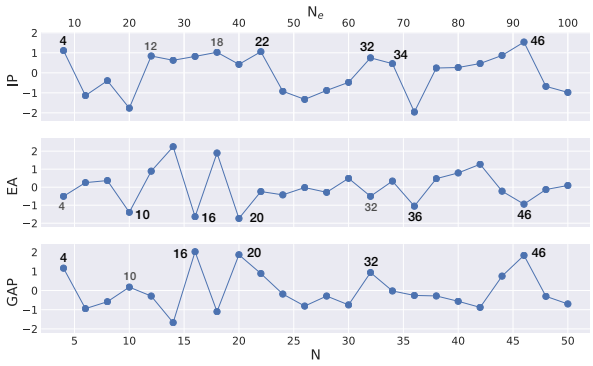

Fig. 5 The standardized vertical ionization energy, electron affinity and fundamental gap are shown as a function of the cluster size N (lower scale) or the number of electrons N_e (upper scale). Relevant cluster sizes are explicitly annotated in the figure, weaker features with a smaller size number.

quantities are shown in tabular form in the ESI†. They all display a steep slope as a function of cluster size which makes it difficult to appreciate relevant local variations. For an optimal visualization, we have processed these indicators in the following way: first, we have fitted the numerical data to cubic polynomial functions in order to remove the global trend in the size evolution; then, we have shifted the mean value of the trendless data to zero and divided them by the standard deviation of the data set. The resulting "standardized" data are dimensionless and are shown in figure 5. Local maxima in E_{gap} identify those clusters that are more electronically stable against both oxidation and reduction processes. A simple spherical jellium model predicts that this should occur for metallic clusters with $N_e = 8, 18, 20, 34, 40, 58, 68-70, 92, \ldots$ electrons. Jellium models allowing for ellipsoidal or arbitrary deformations in the angular shape of the confining potential can predict additional (sub-shell) closings due to the splitting of angular momentum multiplets in a non-spherical potential. In discussing the results of this figure, we first notice that having fixed the nanoalloys composition to equiatomic, and Zn and Mg being divalent elements, the total number of valence electrons increases in steps of 4 electrons from one cluster size to the next, so some of the expected jellium shell closings may not be realized in our data set.

The results in figure 5 demonstrate that equiatomic Zn-Mg nanoalloys still conform with the jellium paradigm quite well, but not as closely as the pure Mg and Zn clusters do, probably as a consequence of the significant charge transfer effects. The most important electron shell closings occur for $N = 4, 16, 20, 32, 46$ atoms, i.e. for $N_e = 8, 32, 40, 64, 92$ electrons, while only a hardly appreciable local maximum is observed for $N = 10$ (20 electrons). Sizes $N = 4, 20$ and 46 ex-

actly coincide with spherical jellium shell closings. Signatures of other spherical shell closings can only be partially or indirectly seen: for example, there is a deep minimum in the electron affinity for $N_e = 20$ electrons which is one of the expected signatures of a significant shell closing, but the corresponding ionization energy is quite low, hence the gap is not especially large in Zn_5Mg_5; although none of our clusters has exactly 34 electrons, the deep minimum in the gap for a cluster with $N_e = 36$ electrons is induced by the opening of a new electron shell; a mild local maximum at $N = 28$ is the only visible signature of the shell closing expected for $N_e = 58$ electrons, again a value not realized in our cluster sample; finally, the sharp decrease in the ionization energy after $N = 34$ is associated with the spherical shell closing expected at $N_e = 70$ electrons.

The enhanced electronic stability of $Zn_{16}Mg_{16}$ is due to its marked oblate deformation, which produces a strong fragmentation of the $2D$ shell in which the levels with $|M| = 2$ are stabilized. Its superatomic electron configuration would be $\ldots 1G^{18}2D^4 3S^2$. Similarly, Zn_8Mg_8 has a wide gap with 32 valence electrons due to its elongated shell (in fact, it is well known that clusters with around 30 electrons are very stable in an ellipsoidal jellium model description if they adopt a prolate shape[41,42]). The prolate distortion destabilizes now the $1F$ orbitals with $|M| = 3$ and additionally stabilizes a lot the $2P_z$ orbital, producing the superatomic configuration $\ldots 2S^2 1F^{10} 2P_z^2$.

We notice that the optimal combination of a large ionization energy together with a low electron affinity only occurs for $N = 4, 32$ and 46, while for all other sizes the IP and EA contributions to the fundamental gap compete, this being the main reason for the difficulties in detecting strongly marked features in the size evolution of the gap. The deep IP minimum obtained for the nanoalloy with $N_e = 20$ electrons represents the most important departure from jellium predictions, although the point is that this cluster is not spherical at all so purely geometric packing effects may be dominating its stability.

3.4 Cluster Stabilities

In order to analyze the size dependence of cluster stabilities, figure 6 shows three different indicators: the cohesive energy (or binding energy per atom) is defined as $E_{coh}(N) = \frac{E(\mathrm{Mg})+E(\mathrm{Zn})}{2} - \frac{E_N}{N}$, where E_N is the energy of the nanoalloy with N atoms; the first-order energy difference $E_{evap}(N)$ is the dissociation energy of a ZnMg formula unit; finally, the second-order energy difference is $\Delta_2(N) = E_{N-2} + E_{N+2} - 2E_N$. The cohesive energy quantifies the total internal energy content of a cluster and is therefore a measure of its global (or absolute) stability. E_{evap} and Δ_2 provide more "local" stability measures, by comparing the energy of a cluster of size N to

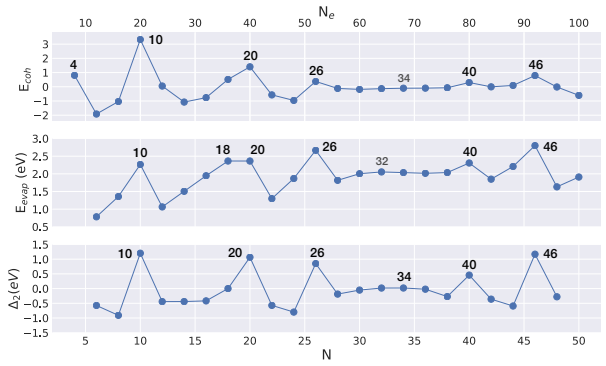

Fig. 6 Size dependent stabilities of equiatomic Zn-Mg nanoalloys are shown as a function of the total number of atoms N (lower scale) or the total number of electrons N_e (upper scale). The upper graph shows the cohesive energies as standardized adimensional quantities. The middle graph shows the energy cost of evaporating (or dissociating) a ZnMg dimer. Finally, the lower graph displays the second-order energy differences. Clusters with enhanced stability (or magic sizes) are explicitly annotated for each of the stability indicators, with a number of smaller size the weaker the corresponding feature.

that of clusters with neighboring sizes. The cohesive energies are shown as standardized adimensional numbers in order to make the local variations more apparent in the figure (the raw cohesive energies are shown in the ESI†). The indicators agree in identifying clusters with $N = 4, 10, 20, 26$ and 46 atoms as the most stable (or magic) sizes, although sizes $N = 40$ and (to a lesser extent) $32 - 34$ also display locally enhanced stabilities of secondary importance.

In our opinion, the most interesting conclusion from the results of figure 6 is that the magic sizes are not so correlated with electronic shell closings as they are in pure Zn and Mg clusters, which we associate again to the non negligible charge transfer effects which introduce an ionic component into the calculation of stabilities. Only the magic numbers $N = 4, 20$ and 46 can be clearly correlated with electronic shell closings. The wide electronic gap observed at $N = 16$ (figure 5) does not result in a specially stable cluster, and the high ionization energy for $N = 32 - 34$ is hardly reflected in the corresponding thermodynamic stabilities.

On the other hand, there are very stable nanoalloys that do not have a specially stable electronic structure ($N = 10, 26, 34, 40$). Their stability must then be associated with other factors, such as geometric packing or an special chemical coordination framework. The number of Zn-Mg heterobonds was the dominating factor in determining the most stable homotop for each separate cluster size, but it is not expected to affect significantly the size dependence of stabilities as essentially all nanoalloys are well mixed (see figure 4). In

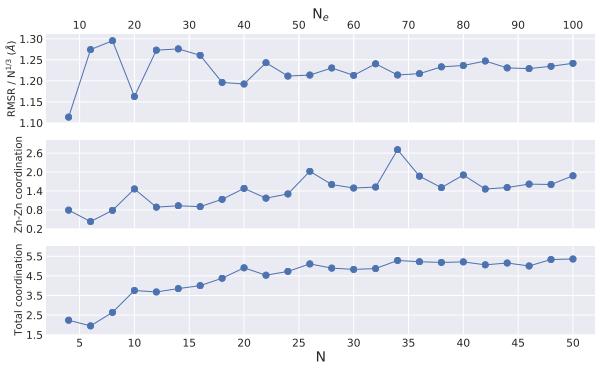

Fig. 7 Upper graph: the root-mean-squared cluster radius, divided by $N^{1/3}$; middle graph: the total number of Zn-Zn bonds per Zn atom; lower graph: the total number of bonds per atom. All the indicators are shown as functions of the total number of atoms (lower scale) or of electrons (upper scale).

searching for meaningful correlations between cluster stabilities and other geometric factors, we have evaluated several descriptors and show the most relevant ones in figure 7. The upper graph shows the root-mean-squared cluster radius divided by $N^{1/3}$ as a measure of the compactness of the nanoalloy structures. It is expected that more compact clusters result from a relatively stronger bonding and so can display some correlation with stabilities[43]. The lower graph shows the average coordination number per atom as a global measure of bond connectivity. Finally, the middle graph displays the average number of Zn-Zn bonds per Zn atom. We have also analyzed the average magnitude of Bader charges as a function of size (not explicitly shown), and observed that the local maxima in the average Zn-Zn coordination generally correlate with cluster sizes displaying an enhanced degree of charge-transfer, although the correlation is not perfect and the few exceptions to it will be explained in the discussion below.

The only indicator that shows a perfect correlation with the unexplained magic numbers is the average Zn-Zn coordination, as it displays clear local maxima for $N = 10, 26, 34$ and 40 atoms. Most of these maxima are reflected in the global coordination (lower graph), although the feature at $N = 40$ is hardly visible in this indicator. Meanwhile, the number of Mg-Mg bonds (not explicitly shown) is not especially high at those sizes (for some of them is even a local minimum), so the enhanced average coordination at those sizes clearly results from an enhanced Zn-Zn coordination. As mentioned above, a complete swap of A and B elements produces an inverted homotop with more Mg-Mg bonds which is significantly less stable than the GM homotop. The upper graph shows that the cluster with $N = 10$ atoms is also significantly more compact than their neighbors, but this indicator does not consistently correlate with the other enhanced stabilities. In summary, our results demonstrate that, all the nanoalloys being similarly well mixed, those with a significantly larger number of Zn-Zn contacts are more stable. As pure Mg is more cohesive than pure Zn, these results are an indirect demonstration of the significant strengthening of Zn-Zn bonds induced by alloying and charge transfer.

We can thus provide a detailed explanation for each of the magic clusters displayed in figure 6. Zn_5Mg_5 is very stable despite not being an electronic shell closing because it satisfies all other requirements for a high stability: it is maximally mixed and has a very compact structure based on the tri-capped trigonal prism unit which is known to be very stable also in pure zinc clusters[6,7]. Additionally, the observed compositional segregation, with Zn atoms exclusively occupying sites of the trigonal prism and Mg atoms occupying all the external capping sites, results in a larger charge transfer contribution to the stability and in a maximization of strengthened Zn-Zn bonds. $Zn_{10}Mg_{10}$ does not just have a very stable closed shell electronic structure and perfect mixing, but additionally figure 7 shows that it satisfies as well the requirements of high structural compactness, bond connectivity, and a larger than average number of Zn-Zn bonds. $Zn_{13}Mg_{13}$ can be considered a geometric shell closing with high symmetry, bond connectivity and a large number of Zn-Zn bonds. Here it is worth mentioning that $Zn_{12}Mg_{12}$ is similarly compact and is more stabilized than size $N = 26$ by charge transfer effects, so size $N = 24$ is less stable than $N = 26$ only because of its significantly lower bond connectivity and smaller number of Zn-Zn bonds. In fact, a direct visualization of the structures in figure 3 already shows that there are several low-coordinated atoms in $Zn_{12}Mg_{12}$, which are not present in $Zn_{13}Mg_{13}$. $Zn_{23}Mg_{23}$ is a purely electronic magic number, as it does not satisfy any of the identified structural criteria for stability. The local stability for $N = 40$ atoms can only be due to having a higher Zn-Zn coordination than the neighboring sizes. Finally, $N = 34$ shows the most important maximum in average Zn-Zn coordination because it has a pure zinc core, but not a very high stability because it is significantly less mixed (figure 4) than other clusters precisely because of the segregation of Zn atoms to the core.

As a final stability indicator, we present in figure 8 the calculated excess energies per atom, defined as:

$$E_{excess}(N) = \frac{1}{N}E(\mathrm{Zn}_{N/2}\mathrm{Mg}_{N/2}) - \frac{1}{2}E(\mathrm{Mg}_N) - \frac{1}{2}E(\mathrm{Zn}_N). \quad (12)$$

The excess energy per atom quantifies the average energy gain upon formation of the nanoalloys from the corresponding pure clusters of the same size. Figure 8 demonstrates that alloying is exothermic for all sizes, with a global decreasing trend so that formation of the nanoalloy is more exothermic the bigger the size. On top of that average trend, the size $N = 26$ clearly

stands out as the one where alloying is most exothermic. The deep minimum in excess energy strongly suggests that the specific combination of two Z16 units is very favorable and is a serious candidate as a building unit in intermetallic bulk ordered phases with close to equiatomic composition which are not characterized yet, as for example $Mg_{12}Zn_{13}$. More in detail, size $N = 24$ produces the second most stable excess energy, and local minima occur for $N = 10, 18$ and 38, i.e. precisely for those sizes displaying either a clear compositional layering ($N = 24, 26, 38$), or another type of strong chemical ordering: for $N = 10$, the ordering is more of a core@shell type, with all Mg atoms occupying more external sites; in $N = 18$, there is an alternance of Zn and Mg elements around the 5-fold axis of the decahedron. From this we can conclude that there is a driving force towards chemically ordered phases in Zn-Mg alloys around the equiatomic composition ratio.

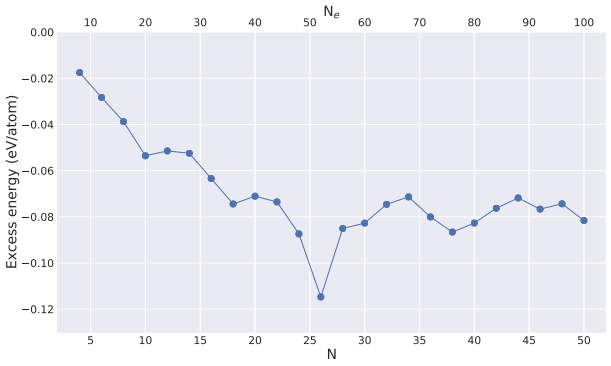

Fig. 8 The excess energy per atom is displayed as a function of cluster size N.

4 Conclusions and Summary

We have developed and presented a new EP model, called Coulomb-corrected-Gupta potential, that should be useful in locating global minimum structures of metallic nanoalloys with a non-negligible degree of charge tranfer, or more in general in simulating materials with both metallic and ionic contributions to bonding. The new potential augments the bare Gupta potential with an explicit ionic interaction model containing monopolar electrostatic interactions between point charges and atomic charging self-energies. Opposite to previous similar works that used EEM-derived charges, our ionic model is feeded with parameterised values of Bader charges of *ab initio* quality, thus ensuring reproduction by the model of the correct charge transfer trends, at a computational cost which is significantly lower than that needed to derive EEM charges. The parameters of the potential are fitted to *ab initio* data generated for a diverse training set of cluster structures. The model is then applied to locate the GM structures of equiatomic Zn-Mg nanoalloys with up to 50 atoms in size within an EP-DFT approach. Our results demonstrate that the Coulomb-corrected-Gupta potential is much superior to the bare Gupta model in its ability to locate stable homotops, allowing to conclude that charge transfer effects are essential for a proper modeling of these materials. In the following we enumerate the more specific conclusions extracted from our work.

We employ an extensive testing set containing around 700 cluster configurations to quantitatively assess our potential models. A somewhat negative conclusion from our work is that charge transfer corrections improve the error of the fitting by a mere 5% as compared to a bare Gupta potential. Large quantitative errors thus remain in the Coulomb-corrected model, of around 0.4 eV/Å in forces and 0.12 eV/atom in binding energies, when compared to *ab initio* results. We conclude that charge transfer effects do not seem to be the main quantitative correction in the search for a very accurate potential. The ionic contribution amounts to a 6% of the total binding energy, which is smaller than initially expected based on the large values of Bader charges. This small contribution results from the scaling down of Bader charges by a factor of 0.28, strictly needed to reproduce the curvature of the *ab initio* potential energy landscape around local minima. Although negative, we consider this is a very interesting conclusion. In future work, we will try to improve the potential model by dispensing with the Gupta description of metallic interactions and using a neural network potential instead.

Notwithstanding the small percentage ionic contribution to the binding energy, the new potential greatly improves the energetic ordering of homotops, allowing to locate much more stable chemical order patterns than the bare Gupta potential, which is the positive aspect of this work. Applicability of our scheme to other materials will depend on the ability to accurately parameterise Bader charges, something that we expect to be feasible in alloys with a substantial degree of charge transfer.

The skeletal atomic structures of equiatomic Zn-Mg nanoalloys are generally similar to those of pure Zn clusters[6,7]. The most stable chemical order is the maximally mixed one for the majority of sizes, with the nanoalloys displaying an additional tendency towards compositional layering. We have identified additional factors of secondary importance that complete the description of chemical order systematics and cluster stability:

- In very small clusters with no core atoms, maximization of Mg-Mg bonds can compete with the dominating maximal mixing rule. So in the very small size range, we conclude that Mg-Mg bonds are stronger than Zn-Zn bonds, as it is the case in the pure metals.

- Size mismatch effects control the chemical composition

of the core in core@shell clusters, and can also compete with the maximal mixing rule. For each core size, the core composition evolves from Zn-rich towards Mg-rich as the cluster size increases.

- Maximization of Zn-Zn contacts (under the constraint of maximal mixing) is observed for clusters with significant charge transfer. In particular, those clusters with a larger than average number of Zn-Zn bonds are found to possess enhanced thermodynamic stability, a correlation that demonstrates that Zn-Zn bonds are significantly strengthened in the alloys due to the charge transfer effects.

We have compared our structural results with the available literature on the bulk Zn-Mg phase diagram. The $Zn_{12}Mg_{12}$ nanoalloy is a fragment of the Pmma bulk lattice, a metastable intermetallic phase predicted computationally for the equiatomic alloy; $Zn_{13}Mg_{13}$ is a fragment of the $R\bar{3}c$ lattice of $Mg_{21}Zn_{25}$, a stable intermetallic phase. Thus a preference for bulk-like structural and chemical orderings, including a clear compositional layering, becomes evident already at quite small sizes.

Both electronic and stability indicators suggest that Zn-Mg nanoalloys conform to a jellium picture of delocalized electrons to a lesser extent than pure Zn or Mg clusters do, as a result of the ionic contribution to bonding due to the charge transfer. Magic clusters with an enhanced stability occur for $N = 4, 10, 20, 26, 34, 40, 46$ atoms. Only a few of them correlate with an electronic shell closing, while others are explained by geometric packing and bond connectivity arguments, in particular by the strengthening of Zn-Zn bonds upon alloying. It is reassuring to observe that the two factors (electronic and geometric) are important in a material displaying two different contributions to bonding. Formation of the nanoalloy from the pure clusters is most exothermic for $N = 26$. In general, the compositional layering is associated with an enhanced excess energy value.

The present work represents an important step towards reliable modeling of Zn-Mg nanoalloys, in which we are interested due to their excellent corrosion protection properties for specific compositions such as $MgZn_2$ or Mg_2Zn_{11}. The observation that small nanoalloys already adopt structural motifs and chemical orderings of bulk phases suggests they might be simple yet meaningful models for simulating chemical processes relevant to realistic anti-corrosion materials. Similarly, the finding that Zn-Zn bonds can be significantly strengthened upon alloying suggests that magnesium atoms may be preferentially attacked by oxygen reagents, promoting surface segregation of Mg atoms under an oxidizing atmosphere and the formation of a magnesium-rich oxide crust, features that have been observed experimentally [1–3]. Future work will focus on obtaining reliable structural and electronic data for Zn-Mg nanoalloys with those two compositions, and on analysing their reactivity when placed in an oxidizing environment. But with more generality, we expect the model proposed here can reveal itself as a useful tool for many other metallic alloys that display significant charge transfer effects.

Conflicts of interest: There are no conflicts of interest to declare.

We gratefully acknowledge the support of the "Junta de Castilla y León" (Project No. VA124G18) and Spanish Ministry of Economy and Competitiveness (Project PGC2018-093745-B-I00).

References

1 Hosking, N. C.; Strom, M. A.; Shipway, P. H.; Rudd, C. D. *Corros. Sci.* **2007**, *49* 3669.
2 Prosek, T.; Nazarov, A.; Bexell, U.; Thierry, D.; Serak, J. *Corros. Sci.* **2008**, *50* 2216.
3 Diler, E.; Rioual, S.; Lescop, B.; Thierry, D.; Rouvellou, B. *Corros. Sci.* **2012**, *65* 178.
4 Velikokhatnyi, O. I.; Kumta, P. N. *Acta Biomater.* **2010**, *6* 1698-1704.
5 Datta, A.; Waghmare, U. V.; Ramamurty, U. *Acta Mater.* **2008**, *56* 2531-2539.
6 Aguado, A.; Vega, A.; Lebon, A.; von Issendorff, B. *Angew. Chem. Int. Ed.* **2015**, *54*, 2111-2115.
7 Aguado, A.; Vega, A.; Lebon, A.; von Issendorff, B. *Nanoscale* **2018**, *10*, 19162-19181.
8 Lebon, A.; Aguado, A.; Vega, A. *Corros. Sci.* **2017**, *124*, 35-45.
9 Ferrando, R.; Fortunelli, A.; Johnston, R. L. *Phys. Chem. Chem. Phys.* **2008**, *10*, 640-649.
10 Zhang, M; Fournier, R. *J. Mol. Struct. (THEOCHEM)* **2006**, *762*, 49-56.
11 Zhang, M; Fournier, R. *J. Phys. Chem.* **2009**, *113*, 3162-3170.
12 Cerbelaud, M.; Ferrando, R.; Barcaro, G.; Fortunelli, A. *Phys. Chem. Chem. Phys.* **2011**, *13*, 10232-10240.
13 R. P. Gupta, *Phys. Rev. B* **1981**, *23*, 6265.
14 V. Rosato, M. Guillopé, B. Legrand, *Philos. Mag. A* **1989**, *59*, 321.
15 Cleri, F.; Rosato, V. *Phys. Rev. B* **1993**, *48*, 22.
16 Pauling, L.: The Nature of the Chemical Bond. Cornell University Press, New York (1960).
17 Louwen, J. N.; Vogt, E. T. C. *J. Mol. Catal. A: Chem.* **1998**, *134*, 63-77.
18 Rappé, A. K.; Goddard, W. A. *J. Phys. Chem.* **1991**, *95*, 3358.
19 Geerlings, P.; De Proft, F.; Langenaeker, W. *Chem. Rev.* **2003**, *103*, 1793-1873.

20 Mortier, W. J.; Ghosh, S. K.; Shankar, S. *J. Am. Chem. Soc.* **1986**, *108*, 4315-4320.
21 Bultinck, P.; Langenaeker, W.; Lahorte, P.; De Proft, F.; Geerlings, P.; Waroquier, M.; Tollenaere, J. P. *J. Phys. Chem. A* **2002**, *106*, 7887-7894.
22 Bultinck, P.; Langenaeker, W.; Lahorte, P.; De Proft, F.; Geerlings, P.; Van Alsenoy, C.; Tollenaere, J. P. *J. Phys. Chem. A* **2002**, *106*, 7895-7901.
23 Sanderson, R. T. *Science* **1951**, *114*, 670.
24 Donnelly, R. A.; Parr, R. G. *J. Chem. Phys.* **1978**, *69*, 4431.
25 Politzer, P.; Weinstein, H. *J. Chem. Phys.* **1979**, *71*, 4218.
26 Manz, T. A.; Sholl, D. S. *J. Chem. Theory Comput.* **2010**, *6*, 2455-2468.
27 López, M. J.; Jellinek, J. *J. Chem. Phys.* **1999**, *110*, 8899.
28 http://www-wales.ch.cam.ac.uk/GMIN/.
29 Wales, D. J.; Doye, J. P. K. *J. Phys. Chem. A* **1997**, *101*, 5111.
30 Wales, D. J.; Scheraga, H. A. *Science* **1999**, *285*, 1368-1372.
31 Soler, J. M.; Artacho, E.; Gale, J. D.; García, A.; Junquera, J.; Ordejón, P.; Sánchez-Portal, D. *J. Phys.: Condens. Matter* **2002**, *14*, 2475.
32 Perdew, J. P.; Burke, K.; Ernzerhof, M. *Phys. Rev. Lett.* **1996**, *77*, 3865.
33 Hamann, R.; Schlüter, M.; Chiang, C. *Phys. Rev. Lett.* **1979**, *43*, 1494.
34 Kleinman, L.; Bylander, D. M. *Phys. Rev. Lett.* **1982**, *48*, 1425.
35 Louie, S. G.; Froyen, S.; Cohen, M. L. *Phys. Rev. B* **1982**, *26*, 1738.
36 Mao, P.-L.; Yu, B.; Liu, Z.; Wang, F.; Ju, Y. *Trans. Nonferrous Met. Soc. China* **2014**, *24*, 2920-2929.
37 Okamoto, H. *J. Phase Equilib. Diff.* **2013**, *34*, 251263.
38 Villars, P.; Calvert, L. K. Pearsons Crystal Data, Crystal Structure Database for Inorganic Compounds, CD-ROM software version 1. 3, OH, 2009.
39 Ghosh, P.; Mezbahul-Islam, M.; Medraj, M. *Calphad* **2012**, *36*, 2843.
40 Persson, K. Materials Data on MgZn (SG:51) by Materials Project. **2016**. doi:10.17188/1315883.
41 Brack, M. *Rev. Mod. Phys.* **1993**, *65*, 677.
42 de Heer, W. A. *Rev. Mod. Phys.* **1993**, *65*, 611.
43 Aguado, A.; Jarrold, M. F. *Annu. Rev. Phys. Chem.* **2011**, *62*, 151.